Applied Surface Science 639 (2023) 158152

Contents lists available at ScienceDirect

Applied Surface Science

journal homepage: www.elsevier.com/locate/apsusc

Full Length Article

Atomic-scale insights into the tribochemical wear of diamond on quartz surfaces

Jagjeevan S. Bhamra [a,*], James P. Ewen [a,b,c,*], Carlos Ayestarán Latorre [a], John A.R. Bomidi [d], Marc W. Bird [d], Daniele Dini [a,b,c]

[a] Department of Mechanical Engineering, Imperial College London, South Kensington Campus, London SW7 2AZ, UK
[b] Institute of Molecular Science and Engineering, Imperial College London, South Kensington Campus, London SW7 2AZ, UK
[c] Thomas Young Centre for Theory and Simulation of Materials, Imperial College London, South Kensington Campus, London SW7 2AZ, UK
[d] Baker Hughes, Houston, TX 77040, USA

ARTICLE INFO

Keywords:
Molecular dynamics
Wear
Nanoscale
ReaxFF

ABSTRACT

A detailed understanding of diamond wear is crucial due to its use in high-performance cutting tools. Despite being a much harder material, diamond shows appreciable wear when cutting silicon dioxides due to a tribochemical mechanism. Here, we use nonequilibrium molecular dynamics simulations with a reactive force field to investigate the wear of single-crystal diamond tips sliding on α-quartz surfaces. Atom-by-atom attrition of carbon atoms is initiated by the formation of C-O interfacial bonds, followed by C-C cleavage, and either diffusion into the substrate or further oxidation to form CO_2 molecules. Water molecules dissociate to form hydroxyl groups, which passivates the surfaces and reduces interfacial bonding and wear. At low loads, the initial wear rate increases exponentially with temperature and normal stress, consistent with stress-augmented thermally activated wear models. At higher loads, the initial wear rate becomes less sensitive to the normal stress, eventually plateauing towards a constant value. This behaviour can be described using the multibond wear model. After long sliding distances, wear also occurs through cluster detachment via tail fracture. Here, wear becomes approximately proportional to the sliding distance and normal load, consistent with the Archard model. The normalised wear rates from the simulations are within the experimentally-measured range.

1. Introduction

Wear mitigation is critical for the long-term reliability, safety, and efficiency of devices containing moving components [1], from artificial hip joints [2] to automotive engines [3]. In most tribological systems, material removal occurs mainly through abrasive wear [4]. The physical and chemical processes leading to wear at sliding interfaces remain quite poorly understood, so the process is usually described empirically [5]. Developed almost seven decades ago, the Archard equation [6] remains the most popular model for abrasive wear inside macroscale contacts [7]. It states that:

$$V = (K_b F_Z d)/H \tag{1}$$

where V is the wear volume, K_b is the wear coefficient, F_z is the load, d is the sliding distance, and H is the material hardness. In tribological systems that follow the Archard equation, wear is thus proportional to F_z and d and inversely proportional to H. The equation was derived from a simplistic physical picture of wear involving plastic deformation of contacting asperities. A large number of experiments are usually required to obtain the wear coefficient, K_b, which hinders the development of low-wear materials [8].

The lack of predictive models for wear and advances in the field of nanotechnology have motivated the detailed study of wear at the atomic level. Several atomic force microscopy (AFM) studies have shown that nanoscale wear cannot be adequately explained using the Archard equation [9–10]. Instead, atom-by-atom attrition occurs, which can be described by a stress-augmented thermally activated (SATA) model [11–12]. In such processes, the wear rate increases exponentially with temperature and applied stress. A non-empirical model for atom-by-atom attrition in nanoscale contacts has also recently been proposed by Wang at al. [8] based on quantities that can be directly obtained from nonequilibrium molecular dynamics (NEMD) simulations. This SATA-based model has been successfully applied to describe the wear of

* Corresponding authors at: Department of Mechanical Engineering, Imperial College London, South Kensington Campus, London SW7 2AZ, UK (James P. Ewen).
E-mail addresses: j.bhamra19@imperial.ac.uk (J.S. Bhamra), j.ewen@imperial.ac.uk (J.P. Ewen).

https://doi.org/10.1016/j.apsusc.2023.158152
Received 3 May 2023; Received in revised form 12 July 2023; Accepted 31 July 2023
Available online 1 August 2023
0169-4332/© 2023 The Author(s). Published by Elsevier B.V. This is an open access article under the CC BY license (http://creativecommons.org/licenses/by/4.0/).

diamond-like-carbon (DLC) contacts in NEMD simulations [8]. Another set of NEMD simulations suggested that, in addition to atom-by-atom attrition, cluster detachment via tail fracture also contributes to wear in DLC contacts, particularly at high loads [13]. These simulations also found that wear increased linearly with normal load and sliding distance [13], which is consistent with the Archard model, but not SATA-based models [6]. Recent nanoscale AFM experiments investigating the wear of DLC-coated tips on DLC substrates have shown that the SATA wear model can also break down under certain conditions [14]. While at low loads, the stress dependence of the wear rate could be described using a SATA model, at higher loads, the wear rate was lower than predicted and eventually levelled out to a constant value. At high loads, wear was essentially proportional to the sliding distance and independent of the normal stress. In rough elastic contacts, where contact area grows linearly with normal load [15], this leads to behavior very similar to that described by the Archard equation. Both of these types of wear behaviour were successfully fitted using a multibond model of single-asperity wear developed by Shao et al., [16] which was based on the multibond friction model due to Filippov et al. [17] that describes friction through the formation and rupture of interfacial bonds. The multibond wear model considers the effects of three competing SATA processes that determine interfacial bond formation, wearless rupture, and the transfer of atoms (i.e. wear) [16].

A detailed understanding of the wear of diamond and other carbon-based materials is important due to their widespread use in high-performance cutting tools [18]. For example, synthetic polycrystalline diamond compact (PDC) drill bits [19] revolutionised the rock drilling industry due to their wide application range, high rate of penetration (ROP), and extended bit life [20]. Accurate prediction of PDC wear is crucial for reducing the number of bit replacements, lowering rig downtime and the large associated economic costs [21]. From the analysis of drilling experiments on a wide range of rock types, Ersoy and Waller concluded that the majority of damage to PDC bits was due to abrasive wear [22]. Consequently, the Archard equation [6] has frequently been used to model the abrasive wear of PDC bits [23–25]. The hardness of the polycrystalline diamond (PCD) used in PDC bits is at least 55 GPa [26]. Operationally, drill bits move through many different types of rocks that have varied and heterogenous mechanical properties. The mean hardness of calcite-rich rocks (e.g. limestone) is only around 2 GPa, while for quartz-rich rocks (e.g. granite) it is between 9 and 15 GPa [26–27]. Since these rocks are much softer than PCD under ambient or typical wellbore temperatures (<300 °C), low abrasive wear rates are expected from the Archard model [6] for PDCs. However, inside the contact, where local cutting temperatures can exceed 750 °C [28], where the effective hardness of PCD can be reduced to below that of granite [29]. Under these accommodating conditions, PDCs are more susceptible to abrasive wear while cutting through granite [30]. Higher PDC wear rates have been observed for granite than limestone [22], as predicted by the Archard model. Indeed, the lifetime of diamond drill bits is generally reduced for rocks with a higher equivalent quartz content [31]. In addition to their high hardness, there may also be a tribochemical component to the high wear rates observed for quartz-rich rocks. It is well known that diamond can be polished with relatively soft silica particles, with the tribochemical mechanism believed to involve the formation of strong C-O bonds across the diamond-silica interface [32]. This hypothesis was recently confirmed by first-principles calculations [33]. Previous experimental studies have also shown that diamond tools exhibit significant wear for the machining of silicon [34], which will form an oxide outer layer when exposed to air. High wear rates have also been observed for diamond tools cutting through soda lime glass [35], whose primary constituent is silica. Significant wear of diamond AFM tips sliding on silicon surfaces has also been observed [36]. However, it is not yet clear to what extent tribochemical wear increases the wear of diamond sliding on crystalline α-quartz surfaces.

In this study, we use NEMD simulations to explore the wear of nanoscale diamond-quartz contacts under high temperature and pressure conditions, which are representative of those experienced during rock drilling. In order to incorporate the effects of interfacial bonding, we employ the reactive force field (ReaxFF) method [37]. The computational cost of MD simulations with ReaxFF are several orders of magnitude lower than first-principle techniques, therefore allowing dynamic evolution of significantly larger systems over larger time scales to be explored [38]. Unlike first-principles methods, ReaxFF requires careful parameterization to ensure validity of chemical reactivity and material properties. In recent years, ReaxFF parameters have been developed for studying a very broad range of systems and processes [39], including a wide range of molecules confined between sliding surfaces to investigate tribochemical processes [40]. In this study, using published ReaxFF parameters for silicon, oxygen, hydrogen, and carbon-containing systems [41], we are able to observe and quantify diamond wear in diamond-quartz contacts, which is initiated by the formation of interfacial bonds between the two surfaces. Using the multibond wear model [16], we can accurately describe the initial wear rate of the diamond tip at realistic bit-rock pressures (2–6 GPa). After the initial running-in period, wear increases approximately linearly with sliding distance and load, which is consistent with the Archard model [6]. These new results complement our previous study that showed diamond-rock friction is governed by interfacial bonding [42]. Collectively, our NEMD simulation results suggest that reducing interfacial bonding could be an effective strategy for reducing both friction and wear during rock drilling.

2. Methodology

2.1. Simulation setup

The mineral distributions in granite rocks display spatial heterogeneity, leading to location-dependent surface chemistry [43]. NEMD simulations paired with ReaxFF are restricted to the studying of nanoscale systems, due to the large computational cost [38]. Therefore, α-quartz, the major constituent of granite [44], was used as a representative model for the rock substrate. The validity of this representation was confirmed in our previous study, where silicon and oxygen were confirmed as the major constituents of the transfer film formed on a diamond pin used in tribometer experiments on granite [42]. The α-quartz {0001} [45] surface has been shown in previous density functional theory studies (DFT) to be the most thermodynamically stable, and therefore was therefore selected for this study. The x, y, z, dimensions of the substrate were 13.7 × 5.8 × 3.7 nm. The tip was modelled by a single-crystal diamond hemisphere with a radius of 2.5 nm [46]. The tip contained 642 carbon atoms, 127 of which were surface atoms. The two systems used in the NEMD simulations (with and without water) are shown in Fig. 1.

Quartz has been shown experimentally to be hygroscopic and expected to be saturated with a water monolayer in both atmospheric and aqueous environments [47]. Consequently, as well as simulating dry surfaces, we also performed NEMD simulations with systems containing 500 water molecules. This was sufficient to fully saturate the α-quartz {0001} surface. Many of the water molecules chemisorbed to the surface during the equilibration phase. As predicted from previous DFT calculations, the chemisorbed water molecules on α-quartz {0001} [48] spontaneously dissociate to form terminal hydroxy groups.

2.2. ReaxFF parameters

ReaxFF is a bond order-based force field that was originally developed by van Duin et al. [49] to investigate the dissociation and reactivity of hydrocarbon molecules. We used the version of ReaxFF implemented in the large atomic/molecular massively parallel simulator (LAMMPS) software [50]. The functional form of ReaxFF used in LAMMPS was outlined by Chenoweth et al. [51] and fully described by Aktulga et al. [52]. The point charges on the atoms vary dynamically during

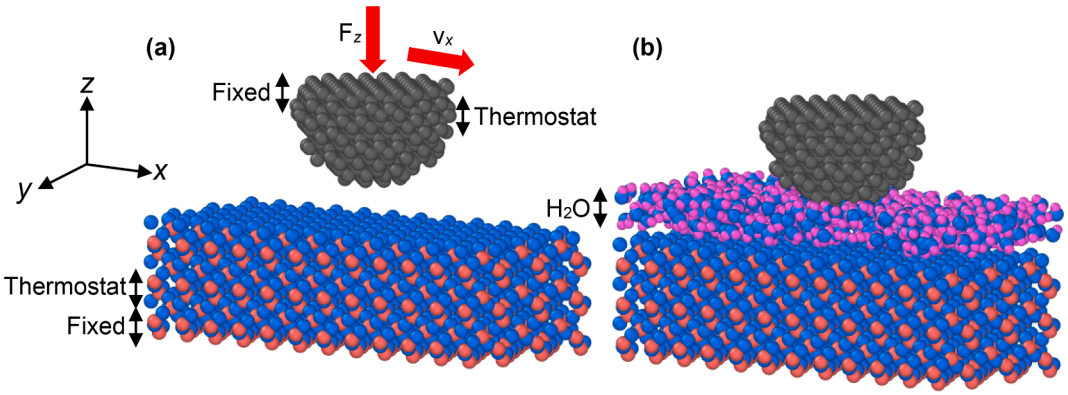

Fig. 1. NEMD systems for the (a) dry and (b) wet (500 H_2O molecules) diamond-quartz systems before equilibration. Silicon atoms are shown in red, oxygen in blue, carbon in grey, and hydrogen in pink. Rendered using OVITO [69]. (For interpretation of the references to colour in this figure legend, the reader is referred to the web version of this article.)

the NEMD simulations and are calculated using the charge equilibration (Qeq) method [52–54].

We used the ReaxFF parameters developed by Newsome et al. [41], which include Si/O/H/C interactions. This force field was originally developed to investigate the oxidation of silicon carbide by oxygen and water and included parameterizations developed from first-principles data for silicon [55], silicon oxides [56–57], and poly(demethylsiloxide) [58]. These ReaxFF parameters predict a heat of formation of −216 kcal mol^{-1} for α-quartz, which is identical to the experimental value. Furthermore, the ReaxFF parameters predict a heat of formation for the SiC-diamond phase of +8 kcal mol^{-1}, in reasonable agreement with the DFT value of + 14 kcal mol^{-1}. The parameters predict heats of formation for CO and CO_2 of −13 and −88 kcal mol^{-1}, respectively, compared with −26 and −94 kcal mol^{-1} from experiment [41]. Thus, the oxidation of the diamond tip is expected to be accurately modelled. The Young's modulus (1024 GPa) and lattice constant (0.362 nm) obtained using this parameter set are close to the experimental values (1065 GPa and 0.357 nm) [59]. The parameters have also been validated against first-principles methods for the interactions between silica surfaces and water molecules [57] and experimental density and bulk moduli of α-quartz {0001} [56]. These parameters have also been successfully applied to study adhesion and interfacial bonding in silicon-diamond [60] and silica-graphene contacts [61], as well as the relationship between interfacial bonding and friction in dry and wet diamond-quartz contacts [42]. The parameters have also shown to satisfactorily reproduce the energy versus strain behaviour from first-principles calculations for C-C bond rupture in hydrocarbons [62]. In a recent comparison of the transferability of interatomic potentials for carbon, ReaxFF was recommended for large systems and long simulation times [63]. ReaxFF has also recently been applied to study the wear of DLC surfaces [8,64]. In summary, the chosen ReaxFF parameter set is deemed suitable for the study of the interfacial C-O bond formation and C-C bond dissociation processes that govern the wear of diamond on quartz surfaces.

2.3. Simulation details

Extreme temperatures (>500 K) and pressures (>200 MPa) are often encountered inside deep wells [65]. During drilling, the local temperature (>800 K) and pressure (>1 GPa) conditions can be even more severe at the bit-rock interface [26]. These extreme conditions complicate the experimental investigation of the friction and wear of new drill bit materials on different rock types [66]. Conversely, these extreme conditions can be directly studied using NEMD simulations.

We performed NEMD coupled ReaxFF simulations using the LAMMPS software package [50]. We used the velocity-Verlet integration algorithm [67] with a time step of 0.25 fs. Periodic boundary conditions were applied in the *x*- and *y*-directions. The bottom atomic layer of the substrate was fixed in the *z*-direction. The temperature was maintained at temperatures ranging from 300 to 1800 K, depending on the system, using a Langevin thermostat [68] with a coupling time of 25 fs. The thermostat was selectively applied to the central layers (in the *z*-direction) of the tip and substrate, as shown in Fig. 1. The thermostat was effective in maintaining the target temperature, even at the high applied sliding velocity (100 m s^{-1}). A reflective boundary was added in the *xy*-plane at the top of the simulation cell (10 nm above the top of the substrate in the *z*-direction) to prevent gaseous species from escaping the simulation box.

The energy of the system was minimized using the conjugate gradient method, followed by equilibration at desired temperature (300–1800 K) for 0.1 ns. During the equilibration, a small constant normal force ($F_n = 1$ nN) was added to the top layer of atoms in the tip to bring it into contact with the substrate. The normal force was then increased to the target value ($F_n = 5$–60 nN) and a sliding velocity in the *x*-direction ($v_x = 100$ m s^{-1}) was added to the top layer of atoms in the tip. The applied normal forces resulted in maximum Hertz pressure in the range $P_{max} = 2.1$–3.0 GPa. Previous simulations have shown that atomic-scale roughness can mean that pressures are significantly underestimated by Hertz theory [70]. Moreover, calculations of pressure with Hertz theory do not account for the increase in contact area and decrease in pressure as the tip geometry flattens due to wear. Therefore, the contact pressures were determined based on the number of atoms in contact, which was quantified through the number of interfacial bonds formed [71–72]. Here, the atoms are assumed to be spherical such that a circular projected area can be defined [71]. The projected area is calculated by multiplying the lattice constant for diamond with our ReaxFF parameterisation (0.362 nm) [59] by the number of atoms in contact [71]. The number of atoms in contact is quantified through the number of interfacial bonds, since previous investigations have shown that only this definition correlates with friction [72]. Since ReaxFF uses a distance-based criterion to calculate the bond order [39], which, in turn, determines whether interfacial bonds form, this method is the essentially the same as using a distance-based criterion with a short cutoff [72]. The atoms in contact method calculated from the number of interfacial bonds resulted in consistently higher pressures than with Hertz theory, in the range $P = 3.7$–5.8 GPa for the dry system and $P =$ 2.1–4.5 GPa for the wet system. A comparison of the pressure as a function of load using Hertz theory and the atoms in contact method based on the number of interfacial bonds can be seen in the Supporting Information (Fig. S1). Both methods predict an approximately linear increase in pressure with load, with the pressure being almost twice as high for the atoms in contact method than Hertz theory, which is due to the larger contact area predicted in the latter case. With an appropriate cutoff distance, distance-based definitions of atomic contact would be

expected to give similar contact areas and pressures to the Hertz estimate, while force-based methods generally lead to larger contact areas and thus lower pressures [72]. A full comparison of the pressures obtained using other possible definitions of atomic contact is beyond the scope of this current study. Wear of the tip means that it becomes increasingly non-spherical, leading to an increase in contact area. This effect is accounted for in the simulations, since the number of atoms in contact is monitored dynamically. The change in pressure from the atoms in contact method over the course of the simulations is shown in the Supporting Information (Fig. S2). Initially, the pressure rapidly drops from very high values (due to the absence of interfacial bonds) and then continues to decrease due to flattening of the tip before reaching a steady-state values after approximately 3 ns. The majority of surface carbon atoms in the tip form interfacial bonds, as shown in the Supporting Information (Fig. S3). There is an increase in the percentage of surface carbon atoms that form interfacial bonds at higher loads, which is due to increased indentation of the tip (Fig. S4), meaning that more of the surface atoms are in contact with the substrate. For all further analyses, unless otherwise stated, we use the steady-state normal stress calculated from the number of atoms in contact [71–72].

To accelerate wear, a high tip sliding velocity of 100 m s^{-1} is applied in all the NEMD simulations. Previous simulation studies have shown that there is negligible difference between the steady-state friction force and interfacial bonding between different sliding velocities (1–10 m s^{-1}) [42]. The compression and sliding phase of the simulations were performed for 4 ns, which was sufficient for friction force and number of interfacial bonds to reach a steady-state. This corresponded to 400 nm sliding distance or approximately 30 surface passes. Chemical bonding information was outputted every 1.0 ps using a bond order cutoff of 0.3 to identify covalent bonds [51]. The choice of bond order cutoff only affects the postprocessing analysis and does not influence the ReaxFF energy or force calculations [73–74].

3. Results and discussion

3.1. Wear behaviour

The number of worn atoms in the NEMD simulations was quantified in two ways. The first method was simply to quantify the number of C-C bonds broken in the diamond tip. The second method was to monitor the number of carbon atoms that formed C-O interfacial bonds, were removed from the asperity though C-C cleavage and either diffused into

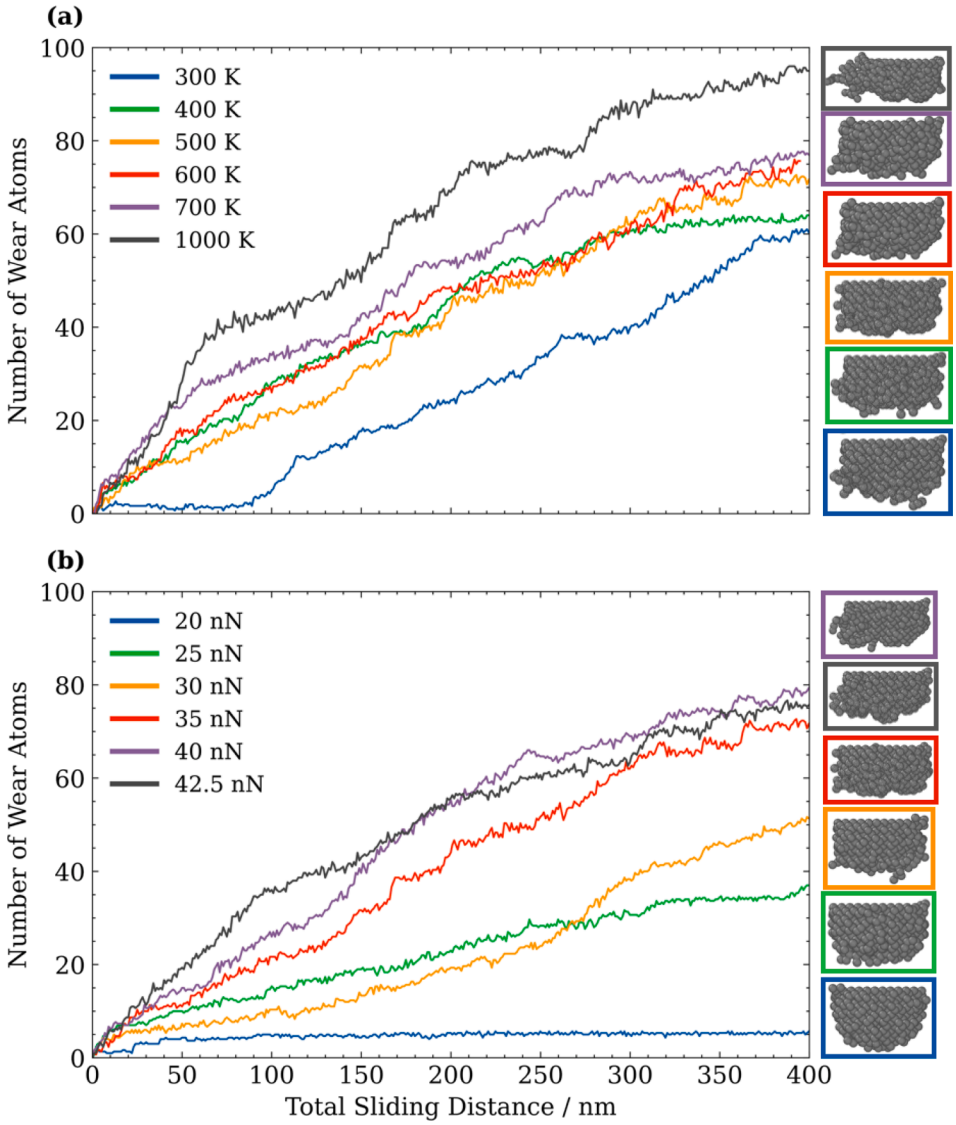

Fig. 2. Change in the number of wear atoms with sliding distance for the dry system at (a) varied temperatures and a constant load of 30 nN (b) varied loads and a constant temperature of 500 K. Worn atoms defined as those that have formed C-O bonds, been removed from the tip through C-C cleavage and diffused into the substrate or oxidised to form CO_2 molecules. Snapshots of the tips after 400 nm of sliding are shown in the coloured boxes.

the α-quartz substrate or were oxidised to form gas-phase CO_2 molecules [75]. The second method is consistent with the definition of wear in recently proposed nanoscale wear models [8,16]. In these models, wear is treated as a multiple-step reaction where interfacial bonds first form between the tip and the substrate, followed by either wearless rupture of the interfacial bond or removal of the bonded atoms by breaking of C-C bonds within the tip. The number of worn atoms using the second method is shown as a function of sliding distance in Fig. 2. Snapshots of the worn tips after 400 nm of sliding are shown in the coloured boxes. Additional snapshots of the tips and substrates after different sliding distances are shown in the Supporting Information (Fig. S4). These snapshots clearly show the diffusion of carbon atoms into the substrate and CO_2 formation. First-principles methods suggest that carbon diffusion through α-quartz requires temperatures in excess of 1000 K; [76] however, the mechanical mixing due to the sliding tip is expected to significantly accelerate this process [77]. Similar wear behaviour is observed when classifying them using the number of C-C bonds broken definition, as shown in the Supporting Information (Fig. S5). This approach includes sp^2-sp^3 transitions within the tip itself (amorphization) [78], which should not themselves be considered as wear since the atoms are not necessarily removed from the tip. Approximately three times as many C-C bonds are broken in the tip (Fig. S5) than contribute to wear (Fig. 2), suggesting that a significant amount of amorphization occurs during sliding. Using both definitions, wear begins from the onset of sliding, suggesting that amorphization is not required to initiate wear. Instead, wear seems to be initiated by the formation of interfacial C-O bonds, which will be studied in the next section. From this point forwards, wear atoms are defined as carbon atoms that have formed interfacial C-O bonds and subsequently been removed from the diamond tip by C-C dissociation, followed by diffusion into the substrate or further oxidation to form CO_2 molecules.

In the Archard model (Equation (1)) [6], the wear volume is expected to increase linearly with the sliding distance, normal force, and hardness. From Fig. 2, there is a sub-linear increase in the number of worn atoms with sliding distance for most of the conditions studied, which is not consistent with the Archard model. This observation is consistent with previous NEMD simulations of silica-silica contacts [79]. Deviations from the Archard model were also observed in previous AFM experiments analysing the wear of silicon tips on a polymer surface [9], silicon-doped DLC tips on silica surfaces [9], and silicon tips on diamond surfaces [11]. The wear volume per unit sliding distance has frequently been found to be non-linearly dependent on the applied load and can also vary with sliding velocity [10,80]. Furthermore, the Archard equation in purely empirical and therefore it remains difficult to extend to elucidate the observations seen in single-asperity wear [9–10,80–81]. These experiments propose that, at the nanoscale, plastic deformation cannot dominate wear, as theorized by the Archard, and instead atom-by-atom attrition takes place. Indeed, *in situ* transmission electron microscopy (TEM) experiments, have shown that silicon tips on a diamond substrate wear without plastic deformation or fracture [11]. The snapshots shown in Fig. S4 confirm that atom-by-atom attrition also occurs in our NEMD simulations.

The initial wear rate (first 100 nm of sliding) in our NEMD simulations shows a significant increase with both temperature (Fig. 2a) and load (Fig. 2b). The maximum temperature considered in our simulations is well below the critical temperature observed in previous NEMD simulations of diamond-titanium contacts above which the mechanical strength of diamond was significantly deteriorated and the tip underwent rapid wear (~2500 K) [82]. The hardness of diamond is only expected to decrease by around 20% between 300 and 1000 K [83]. Thus, from the Archard model, a 20% increase in wear volume would be expected over the temperature range simulated for the dry system. However, the initial wear rate increases by several orders of magnitude between 300 K and 1000 K, as shown in Fig. 2a. Moreover, Fig. 2b shows that the increase in initial wear rate with normal load is super-linear. These observations are both inconsistent with the Archard model. The number of wear atoms as a function of the product of the sliding distance and total normal load is shown in the Supporting Information (Fig. S6); this relationship is neither linear nor consistent across the different loads [11]. Collectively, these observations further suggest that the initial wear of diamond on α-quartz cannot be adequately described by the Archard model.

A sub-linear relationship between initial wear and sliding distance is also observed for the water-containing system, as shown in the Supporting Information (Fig. S7). The temperature and load dependencies of wear are also inconsistent with the Archard model. Compared to the dry systems (Fig. 2), the amount of wear atoms was much lower for the wet systems. Indeed, measurable wear was only detected in the NEMD simulations for the wet system at high temperatures (≥1000 K). Previous experiments by Bowden and Scott [84] also showed that diamond wear on silica glass was greater by two orders of magnitude in a dry atmosphere than in a humid one.

Over the final 300 nm of sliding, the number of wear atoms increases approximately linearly with sliding time. Moreover, wear seems to be less dependent on temperature and load than for the initial 100 nm of sliding. In the following sections, we analyse the wear behaviour in two phases. The initial 100 nm of sliding where the wear rate is higher and the wear versus sliding distance behaviour is strongly sub-linear is referred to as the running-in phase. The following 300 nm of sliding where the wear versus sliding distance becomes more linear (Archard-like) is referred to the steady-state phase.

3.2. Bond formation and cleavage

To identify the physicochemical mechanisms leading to wear, we analysed the key bond formation and cleavage processes at different temperatures and loads. Fig. 3 shows the number of C-O interfacial bonds formed (green), C-O interfacial bonds broken leading to wearless rupture (red), and C-C bonds broken leading to wear (purple) as a function of sliding time at constant load (30 nN) and varied temperature (300–1000 K) for the dry system. The number of interfacial C-Si bonds formed during the NEMD simulations is negligible compared to the number of interfacial C-O bonds, so these are not included in our analysis.

For most of the conditions studied, the C-O interfacial bond formation and C-C wear processes begin simultaneously from the onset of sliding. At 300 K, C-O interfacial bonding occurs from the onset of sliding, but there is a short (1 ns) induction period before wear occurs. This observation implies that wear is initiated by the formation of interfacial C-O bonds. Previous first-principles calculations have shown that wear of diamond on silica is initiated by the mechanochemical activation of C-C bonds by the formation of strong C-O interfacial bonds [33]. The amount of C-O interfacial bond formation and C-O and C-C bond breaking increase rapidly at the start of the simulations before approaching a steady-state value. The initial rate of all three processes increases with temperature. The steady-state number of C-O interfacial bonds broken and formed remains approximately constant over the temperature range studied, since this is mostly governed by the surface area of the tip rather than the conditions.

For the water-containing systems (Fig. S8), significant C-C bond breaking and C-O bond formation was only observed at temperatures>1000 K. The presence of water at the interface leads to passivation of both quartz and diamond to the formation of surface hydroxyl groups rather than interfacial bonds. With hydroxyl passivation of both the tip and substrate, the rate of C-C wear bond breaking and C-O interfacial bond formation and breaking (Fig. S8) are significantly reduced. Previous NEMD simulations using ReaxFF [85] have shown that, at the interface between hydroxylated amorphous silica and oxidized silicon, the degree of atom transfer is substantially reduced when sufficient water molecules are present to form a complete monolayer. This was attributed to silicon atoms at the sliding interface becoming terminated with hydroxyl groups rather than interfacial bonds

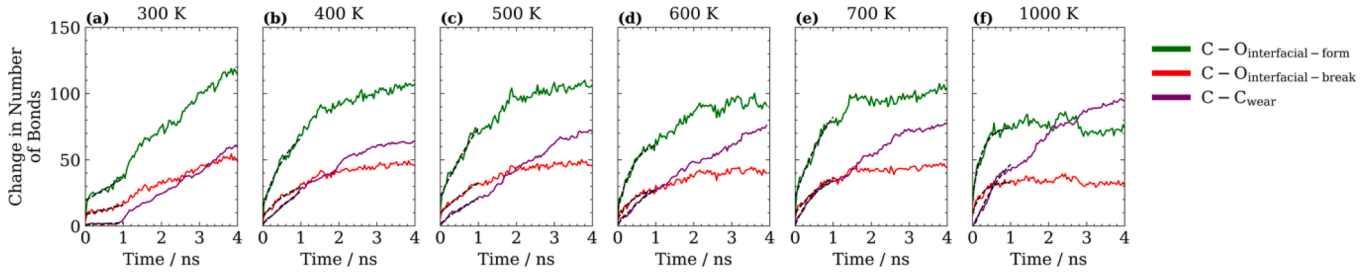

Fig. 3. Number of C-O interfacial bonds formed (green), C-O interfacial bonds broken (red), and C-C wear bonds broken (purple) during sliding for the dry system at a 35 nN load and temperatures of (a) 300 K, (b) 400 K, (c) 500 K, (d), 600 K, (e) 700 K, and (f) 1000 K. Black dashed lines are fits to the first 1 ns of the bond formation/breakage data assuming first-order reactions used to calculate initial rates. (For interpretation of the references to colour in this figure legend, the reader is referred to the web version of this article.)

[85]. Previous NEMD simulations have also shown that friction between silica surfaces [86] and diamond-quartz contacts [42] can be reduced by increasing the hydroxyl group density or adding water molecules between the sliding surfaces. This observation has also recently been recently corroborated for diamond-silica contacts using first-principles methods [87].

Fig. 4 shows the change in the number of C-O interfacial and C-C wear bonds at constant temperature (500 K) and varied load (20–42.5 nN) for the dry system. The steady-state number of C-O interfacial bonds formed and broken, as well as C-C wear bonds broken, increase significantly with increasing load. The steady-state values are also reached at a higher rate as the load is increased. The addition of water molecules at the sliding interface (Fig. S9) leads to a reduction in C-O interfacial bonds formed and C-C wear bonds broken, despite the higher temperature (1000 K) than for the dry systems (500 K).

3.3. Wear models (running-in)

Changes in the wear rate are usually observed shortly after the start of sliding contact between fresh, unworn solid surfaces. The initial period of (usually higher) wear is known as running-in [88]. The running-in phase often determines the subsequent steady-state friction and wear characteristics by complex interfacial pre-conditioning through processes including changes in morphology, tribochemical reactions, tribofilm formation, and structural transformations [89]. Thus, it is important to understand during the running-in as well as the steady-state phase of the wear process.

Initial rates for these bond formation and breaking processes are calculated during the running-in phase, i.e. the first 1 ns (100 nm) of sliding. In many cases, the fits to the initial wear rate data could be extended over the entire 4 ns (400 nm). The initial rate of interfacial C-O bond formation and C-C wear increase with temperature (Fig. 3) and load (Fig. 4). To assess whether these processes can be described with a SATA model [90], we plot the change in the initial rate of C-C wear and interfacial C-O bond formation and breaking against pressure (Fig. 5) and temperature (Fig. 6). The initial rates are calculated over the first 1 ns from the black dotted lines shown in Fig. 3 and Fig. 4, in which C-O formation and C-C cleavage are treated as first-order reactions. In SATA process, the rate constant of the process, k, can be given by:

$$k = A\exp\left(-\frac{\Delta U - N\sigma\Delta V^{\ddagger}}{RT}\right) \quad (2)$$

where A is a pre-exponential factor, ΔU is the activation energy, N is Avogadro's number, σ is the applied stress, $\Delta V^{\ddagger}$ the activation volume, R the universal gas constant, and T is the absolute temperature [90]. Equation (2) implies an exponential increase in the rate with increased applied stress [90], as seen in Fig. 5. The slope of the insets is used to determine $\Delta V^{\ddagger}$. The most appropriate stress component in Equation (2) will depend upon the applied force, materials studied, and geometry of the interface. For the mechanochemical decomposition of lubricant additives, [91] and the oligomerisation of hydrocarbons, [92] the shear stress has been shown to dominate the rate of the process. Some previous nanoscale wear studies have also selected the shear stress as the key parameter [9]. However, most previous studies have used the normal stress (pressure), mostly because it is easier to measure and control [90]. For simplicity and consistency with previous nanoscale wear models [8,16], we also use the normal stress in Equation (2). This was determined using the number of atoms in contact based on the number of interfacial bonds [71].

Fig. 5 shows that the initial rate of C-C bond breaking leading to wear, interfacial C-O bond formation, and interfacial C-O bond breaking (wearless rupture) increase exponentially with pressure, as predicted with SATA models [90]. These observations are consistent with previous experiments and NEMD simulations of dry silica-silica contacts [93]. The slopes of the linear fits in the insets in Fig. 5, yield activation volumes for C-C wear of $\Delta V^{\ddagger} = 1.4 \pm 0.1$ Å^3 for the dry system at 500 K and $\Delta V^{\ddagger} = 1.3 \pm 0.1$ Å^3 and the wet system at 1000 K. This suggests that the normal stress-dependence of wear is similar for the wet and dry systems. The activation volumes calculated from Fig. 5a for C-C wear are consistent with single atom or bond dimensions and are of similar

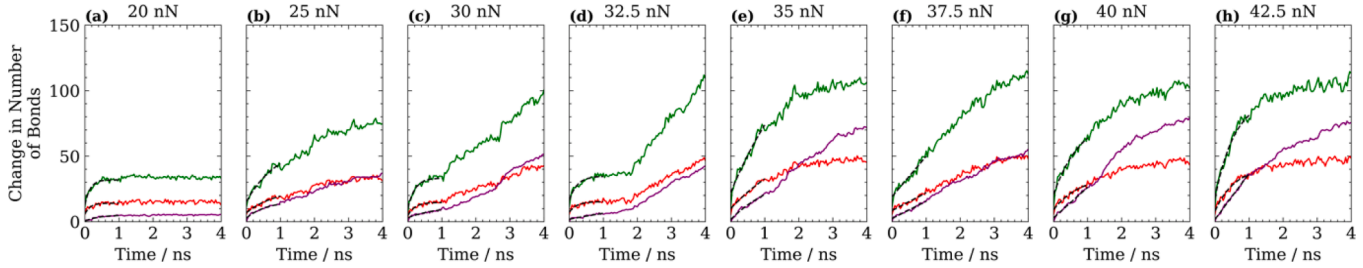

Fig. 4. Number of C-O interfacial bonds formed (green), C-O interfacial bonds broken (red), and C-C wear bonds broken (purple) during sliding for the dry system at 500 K and loads of (a) 20 nN, (b) 25 nN, (c) 30 nN, (d) 32.5 nN, (e) 35 nN, (f) 37.5 nN, (g) 40 nN, and (h) 42.5 nN. Black dashed lines are fits to the first 1 ns of the bond formation/breakage data assuming first-order reactions used to calculate initial rates. Legend same as in Fig. 3. (For interpretation of the references to colour in this figure legend, the reader is referred to the web version of this article.)

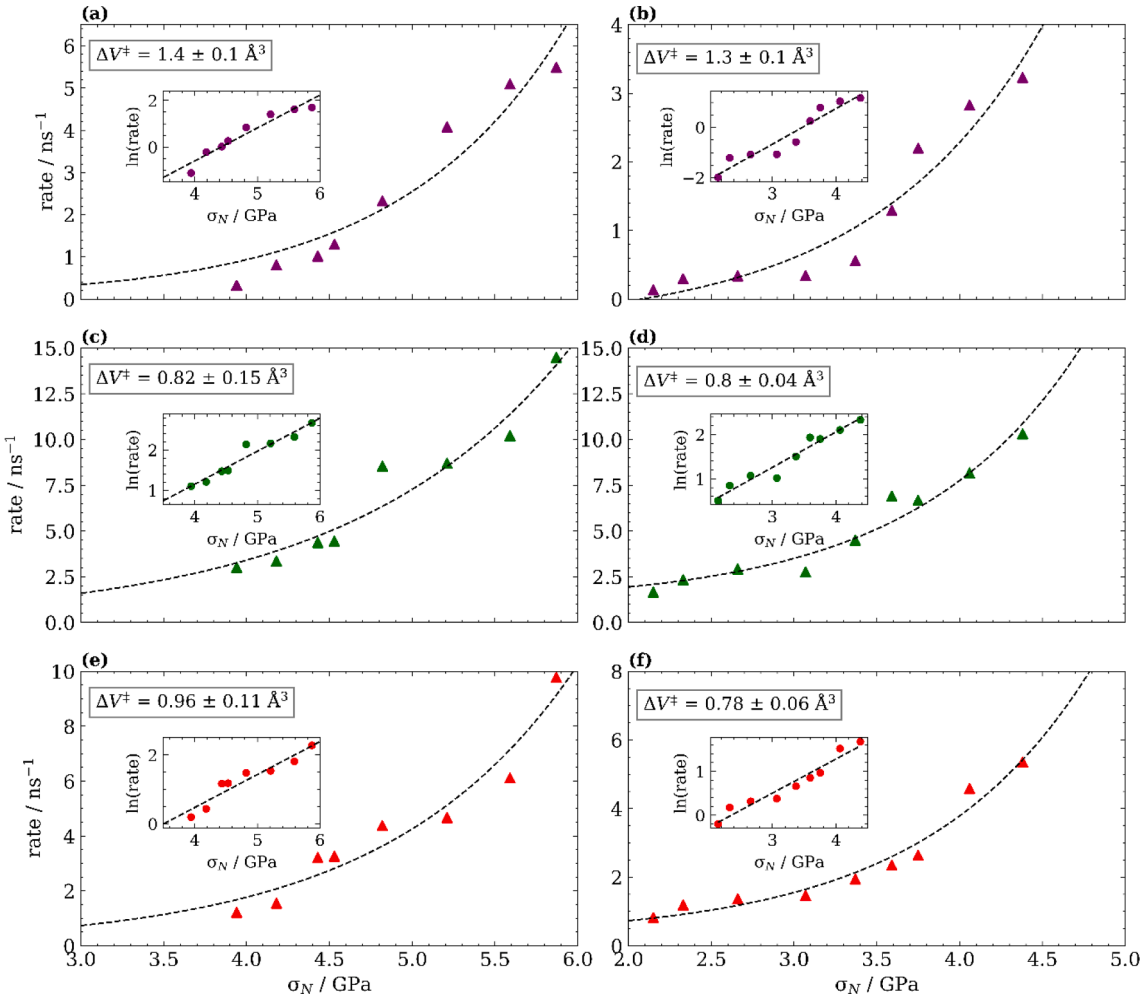

Fig. 5. Change in the initial rate of C-C wear in the dry (a) and wet (b) system, interfacial C-O bond formation in the dry (c) and wet (d) system, and interfacial C-O bond breaking in the dry (e) and wet (f) system with pressure. Pressure calculated using atoms in contact method based on the number of interfacial bonds. Dry systems $T = 500$ K, wet systems $T = 1000$ K. The dashed lines are exponential fits to the data used to calculate the activation volume, $\Delta V^{\ddagger}$, using Equation (2). Insets show the same data with a logarithmic y-axis.

magnitude to those from previous AFM experiments of wear in silica-silica contacts ($\Delta V^{\ddagger} = 6.7 \pm 0.3$ Å^3) [11], DLC-diamond contacts ($\Delta V^{\ddagger} = 5.5 \pm 0.8$ Å^3) [94], and oxidized DLC-silica contacts ($\Delta V^{\ddagger} = 10.8 \pm 0.2$ Å^3) [89]. The values calculated for C-C cleavage are somewhat lower than the activation volume for the graphitization of diamond at high temperature (1580–2280 K) and pressure (0–4.8 GPa) in vacuum ($\Delta V^{\ddagger} = 16.6$ Å^3) [95]. This implies that the C-C cleavage process in sliding diamond-quartz contacts is distinct from the high-temperature, high-pressure graphitization of diamond. Given that the volume of a single carbon at is approximately 2 Å^3, the activation volumes from our NEMD simulations suggests that the effect of the stress on the reaction is localised to single carbon atoms or C-C bonds. On the other hand, for previous experiments of the high-temperature, high-pressure graphitization of diamond, the applied stress likely influences the collective motion of a cluster of around eight carbon atoms [96]. At high pressure, the initial rate of C-C wear stops increasing exponentially with normal stress and approaches a constant value for both the dry (Fig. 5a) and wet (Fig. 5b) systems. This implies that standard SATA wear models [11] are not able to describe the wear behaviour at high loads.

For C-O interfacial bond formation, the activation volume was $\Delta V^{\ddagger} = 0.8 \pm 0.2$ Å^3 for the dry system and $\Delta V^{\ddagger} = 0.8 \pm 0.1$ Å^3 for the wet system, while for C-O interfacial bond breaking, $\Delta V^{\ddagger} = 1.0 \pm 0.1$ Å^3 for the dry system and $\Delta V^{\ddagger} = 0.8 \pm 0.1$ Å^3 for the wet system. Thus, the values for C-O interfacial bond formation and rupture are also consistent with single atom or bond dimensions. The smaller activation volumes suggest these processes are less sensitive to normal stress compared to C-C wear. We also plotted the same data as shown in Fig. 5 but with the normal stress determined using the Hertz equation, as shown in the Supporting Information (Fig. S10). The activation volumes are 16–50% larger when the Hertz equation is used to calculate the normal stress instead of the atoms in contact method based on the number of interfacial bonds, as shown in Table 1.

Fig. 6 shows the exponential increase in the initial rate of C-C bond breaking leading to wear, C-O interfacial bond formation, and C-O interfacial bond breaking, with temperature. The activation energy, ΔU, of these processes was calculated using Equation (2) from slopes of the linear fits in Fig. 6 and the $\Delta V^{\ddagger}$ from Fig. 5. The pre-exponential factor was taken as 10^{13} s^{-1} based on atomic vibration frequencies [89]. For C-C wear, $\Delta U = 71 \pm 3$ kJ mol^{-1} and $\Delta U = 133 \pm 7$ kJ mol^{-1} for the dry and wet systems, respectively. These values are in reasonable agreement with those calculated from previous AFM experimental studies, for example: $\Delta U = 88 \pm 6$ kJ mol^{-1} for wear in silica-silica contacts [11], $\Delta U = 77 \pm 77$ kJ mol^{-1} for wear in oxidized DLC-silica contacts [89], and $\Delta U = 56 \pm 9$ kJ mol^{-1} for wear in DLC-diamond contacts [94]. In previous NEMD simulations of dry DLC-DLC contacts, the activation energy for C-C interfacial bond formation was $\Delta U = 3$ kJ mol^{-1}, while $\Delta U = 87$ kJ mol^{-1} for C-C cleavage [8]. Previous experiments have

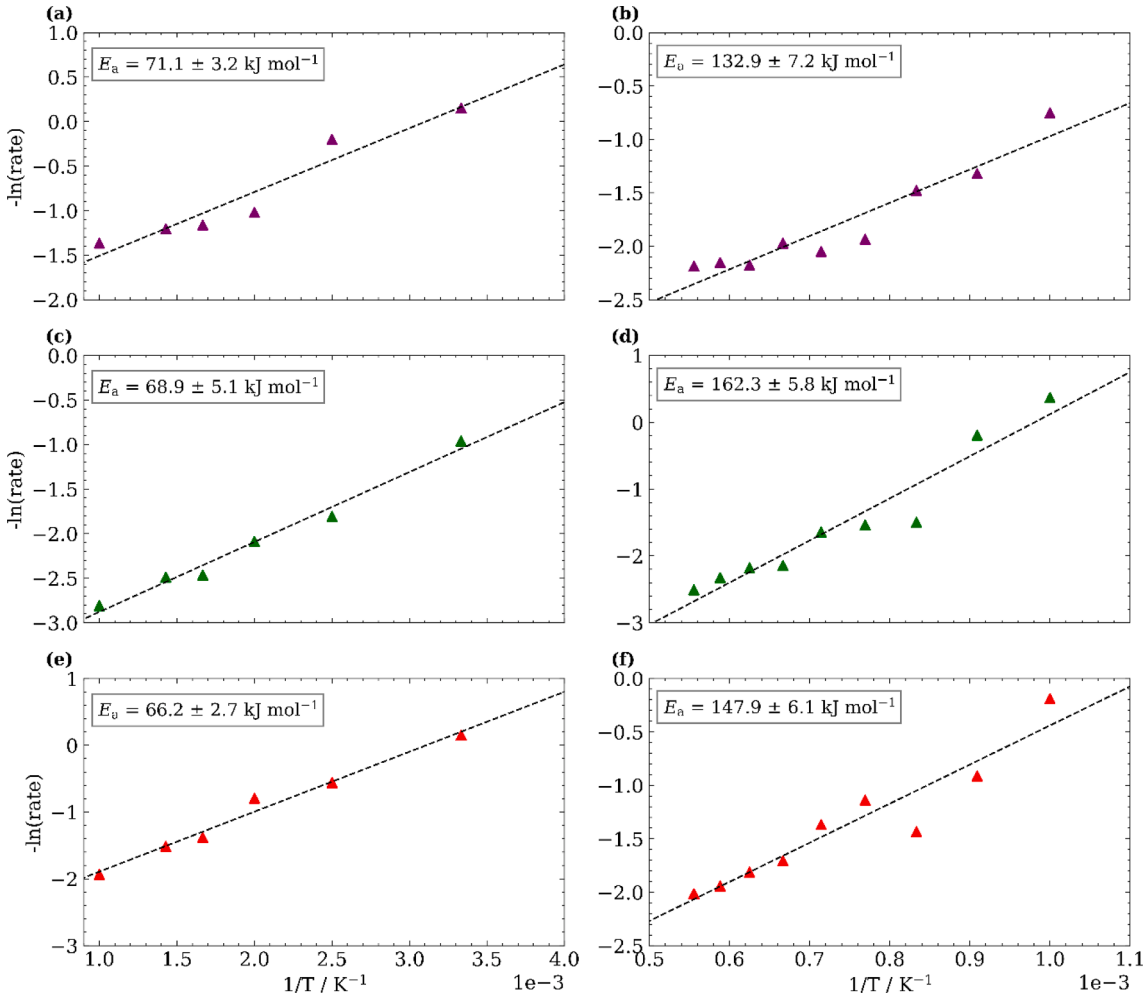

Fig. 6. Change in the initial rate of C-C wear in the dry (a) and wet (b) system, interfacial C-O bond formation in the dry (c) and wet (d) system, and interfacial C-O bond breaking in the dry (e) and wet (f) system, with temperature at a constant load of 35 nN. The dotted lines are exponential fits to the data used to calculate the activation energy, ΔU, using Equation (2).

shown that the activation energy for the graphitization of diamond powder increases with average grain size from $\Delta U = 202$ kJ mol^{-1} for 5 nm to $\Delta U = 365$ kJ mol^{-1} for 35 μm, which is close to the bond dissociation energy of C-C bonds in diamond (367 kJ mol^{-1}) [97]. Therefore, for the single-crystal diamond tip used in the NEMD simulations (radius = 2.5 nm), the α-quartz surface must significantly reduce the activation energy required for C-C bond cleavage.

For C-O interfacial bond formation, the fits in Fig. 6 give $\Delta U = 69 \pm 5$ kJ mol^{-1} for the dry system and $\Delta U = 162 \pm 6$ kJ mol^{-1} for the wet system. The activation energy for diamond oxidation to form CO_2 is around 200 kJ mol^{-1} [98]. For amorphous carbon, which is formed in the NEMD simulations during sliding, the activation energy for oxidation is reduced to approximately 130 kJ mol^{-1} [99]. Thus, the activation energy values from our NEMD simulations are consistent with those measured experimentally for the oxidation of disordered carbon. For interfacial C-O bond breaking (wearless rupture), $\Delta U = 66 \pm 3$ kJ mol^{-1} for the dry system and $\Delta U = 148 \pm 6$ kJ mol^{-1} for the wet system. The presence of water increases the activation energy for all the processes studied, which is due to passivation of the sliding interface through the formation of surface hydroxyls [87]. The activation energies are approximately 20% larger when the Hertz equation is used to calculate the normal stress rather than the atoms in contact method based on the number of interfacial bonds, as shown in Table 1.

We also fit our NEMD data using the non-empirical wear model proposed by Wang et al. [8]. In this method, a nanoscale wear event consists of two steps. Firstly, under load, the contact surfaces are compressed together and react, forming interfacial bonds as an intermediate state in the wear event. The second step consists of atoms involved in the interfacial bonding are sheared and removed from each respective surface, which then leads to wear. This can be considered as a two-step SATA reaction, where interfacial bonding is assisted through normal stress and removal of atoms is assisted by shear stress. Combining reaction rate theory with this two-step reaction, the following non-empirical wear model was proposed:

$$N_{ib} = \frac{2}{A_{atom}} \exp\left(-\frac{\Delta U_{ib} - W_\sigma}{k_B T}\right) \exp\left[\frac{V_{atom}}{2Ek_BT}\left(\frac{F_N}{A_{rc}(F_N)}\right)^2\right] A_{rc}(F_N) \tag{3}$$

$$N_{wear} = \frac{2f_0 t}{A_{atom}} \exp\left(-\frac{\Delta U_{ib} + \Delta U_{wear} - W_\tau}{k_B T}\right) \exp\left[\frac{V_{atom}}{2Ek_BT}\left(\frac{F_N}{A_{rc}(F_N)}\right)^2\right] A_{rc}(F_N) \tag{4}$$

where N_{ib}, is the number of surface atoms that have one or more interfacial chemical bonds, and N_{wear} is the number of worn atoms. Here, ΔU_{ib} and ΔU_{wear} are the only fitting parameters, which represent the activation energies of interfacial bond formation and the removal of carbon atoms that have formed interfacial bonds, respectively [8]. W_σ and W_τ are the external work per atom induced by normal stress, σ, and shear stress, τ. A_{atom} is the surface area per atom, k_B is the Boltzmann

Table 1
Comparison of parameters obtained for the various models using the Hertz equation and atoms in contact method to calculate the contact area and normal stress.

Parameter		Atoms in contact	Hertz Equation
Extracted from the simulations			
$\Delta V^{\ddagger}_{C-O}$ interfacial − form	Dry	0.8 Å^3	1.2 Å^3
$\Delta V^{\ddagger}_{C-O}$ interfacial − break		1.0 Å^3	1.4 Å^3
$\Delta V^{\ddagger}_{C-C}$ wear		1.4 Å^3	2.2 Å^3
$\Delta E_{C-O\,interfacial-form}$		69 kJ mol^{-1}	84 kJ mol^{-1}
$\Delta E_{C-O\,interfacial-break}$		66 kJ mol^{-1}	87 kJ mol^{-1}
$\Delta E_{C-C\,wear}$		71 kJ mol^{-1}	92 kJ mol^{-1}
$\Delta V^{\ddagger}_{C-O}$ interfacial − form	Wet	0.8 Å^3	1.1 Å^3
$\Delta V^{\ddagger}_{C-O}$ interfacial − break		0.8 Å^3	1.0 Å^3
$\Delta V^{\ddagger}_{C-C}$ wear		1.3 Å^3	2.0 Å^3
$\Delta E_{C-O\,interfacial-form}$		162 kJ mol^{-1}	188 kJ mol^{-1}
$\Delta E_{C-O\,interfacial-break}$		148 kJ mol^{-1}	169 kJ mol^{-1}
$\Delta E_{C-C\,wear}$		133 kJ mol^{-1}	153 kJ mol^{-1}
Fitting parameters for multibond model			
ΔE_{on}	Dry	69 kJ mol^{-1}	84 kJ mol^{-1}
ΔE_{off}		66 kJ mol^{-1}	87 kJ mol^{-1}
ΔE_{wear}		71 kJ mol^{-1}	92 kJ mol^{-1}
$\Delta V^{\ddagger}$		1.4 Å^3	2.2 Å^3
ΔU		69 kJ mol^{-1}	84 kJ mol^{-1}
ΔE_{on}	Wet	162 kJ mol^{-1}	188 kJ mol^{-1}
ΔE_{off}		148 kJ mol^{-1}	169 kJ mol^{-1}
ΔE_{wear}		133 kJ mol^{-1}	153 kJ mol^{-1}
$\Delta V^{\ddagger}$		1.3 Å^3	2.0 Å^3
ΔU		162 kJ mol^{-1}	188 kJ mol^{-1}

constant, V_{atom} is volume per atom, E is the Young's Modulus of the contact material, f_0 is the attempt frequency factor, t is sliding time, and $A_{rc}(F_N)$ is real contact area, which is a function of the applied normal load (F_N). Fig. 7 shows the change in N_{ib} (a) and N_{wear} (b) change with normal force at different simulation times for the dry system. Below 30 nN, Equation (3) and Equation (4) can be used to describe the increase in N_{ib} and N_{wear} with load. At higher loads, N_{ib} and N_{wear} level off towards constant values, which cannot be described by the model due to Wang et al. [8]. The same relationship is shown for the wet system in the Supporting Information (Fig. S11). For the wet system, the model does not provide a satisfactory fit to the data even at lower loads.

Changes in the wear behaviour with load have also been observed in previous experiments and simulations. From the results of their NEMD simulations, Yang *et al.* [100] suggested that an atomic-to-plastic wear transition occurs, with SATA models suitable for low loads and the Archard model suitable at high load. Shao et al. [16] noted the same behaviour, but instead attributed the crossover to changes to the relative rates of competing tribochemical phenomena.

We also fit our NEMD data using the multibond wear model due to Shao et al. [16], as shown in Fig. 8. Here, three separate SATA processes are considered. Firstly, bonding occurs between the asperity and substrate by overcoming the energy barrier ΔE_{on}. Next, either these newly formed interfacial bonds break as sliding occurs and the atoms remain bound to the tip (ΔE_{off}) or bonds within the tip break and atoms are transferred across the interface (ΔE_{wear}). In the model the rates of bond formation and rupture are governed by SATA processes, such that:

$$r_{on} = \omega_0 \exp\left(-\frac{\Delta E_{on}}{k_B T}\right) \tag{5}$$

$$r_{off} = \omega_0 \exp\left(-\frac{\Delta E_{off}\left(1-\frac{f_i}{f_c}\right)^{\alpha}}{k_B T}\right) \tag{6}$$

where ω_0 is the atomic attempt frequency (10^{13} s^{-1}), f_i is the tension in each bond and disappears when it reaches a critical value, f_c, and α is set at $\frac{3}{2}$, which is in accordance with the "ramped creep" condition. The model encapsulated a third SATA process, wear, which can be considered as an additional competing rate process, along with r_{on} and r_{off}, such that:

$$r_{wear} = \omega_0 exp\left(-\frac{\Delta E_{wear}\left(1-\frac{f_i}{f_w}\right)^{\alpha}}{k_B T}\right) \tag{7}$$

where f_i is the tension in the bond and f_w is the critical force for a wear event. The outcome of an interfacial bond can either be wearless rupture of the bond, described by r_{off}, or a wear event resulting in atom transfer, r_{wear}. The expected wear rate per potential bonding site is expressed as:

$$\Gamma = -\int_0^{\infty}\left(\frac{r_{wear}}{r_{off}+r_{on}}\right)\left(\frac{n_{on}v}{\Delta x}\right)\left(\frac{dP(\Delta x)}{d\Delta x}\right)d\Delta x \tag{8}$$

where v is the sliding velocity, $P(\Delta x)$ is the probability of a particular bond stretching to a distance less than Δx, and r_{on}, r_{off} and r_{wear} represent the rates of bond formation, wearless rupture, and the transfer of atoms, described by ΔE_{on}, ΔE_{off} and ΔE_{wear}, respectively. Here, n_{on} denotes the fraction of potential bonding sites that are currently bonded. In steady-state, $n_{on} = r_{on}/(r_{on} + r_{off} + r_{wear})$. A full description and mathematical derivation of the model was given by Shao et al. [16]. The normal stress, σ, is not employed as an explicit parameter and instead assumed that the activation energy of bond formation, $\Delta E_{on} = \Delta U - \sigma\Delta V^{\ddagger}$, where ΔU is the activation energy and $\Delta V^{\ddagger}$ is the activation volume of interfacial bond formation (0.8 Å^3), is linearly dependent on normal stress. The normalized wear rate is plotted against a function of dimensionless effective normal stress, $\tilde{\sigma}$, which is inferred from ΔE_{on} and ΔU via:

$$\tilde{\sigma} \equiv \frac{\sigma\Delta V^{\ddagger}}{\Delta U} = 1 - \frac{\Delta E_{on}}{\Delta U} \tag{9}$$

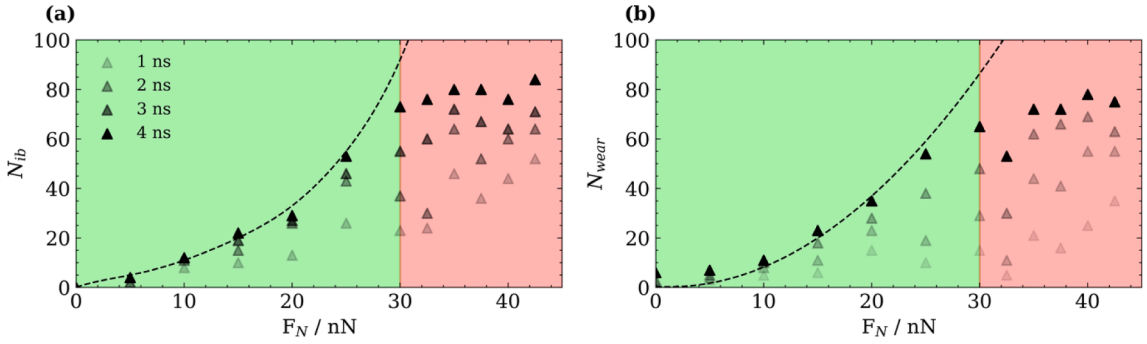

Fig. 7. Change in the number of interfacial bonds, N_{ib}, (a) and number of wear atoms, N_{wear}, (b) with normal load F_N at different simulation times for the dry system at 500 K. Dashed line is fit to Equation (3) in (a) and Equation 4[8] in (b) for the NEMD simulation data after 4 ns up to loads of 30 nN. Green region shows the load range where the model is applicable. (For interpretation of the references to colour in this figure legend, the reader is referred to the web version of this article.)

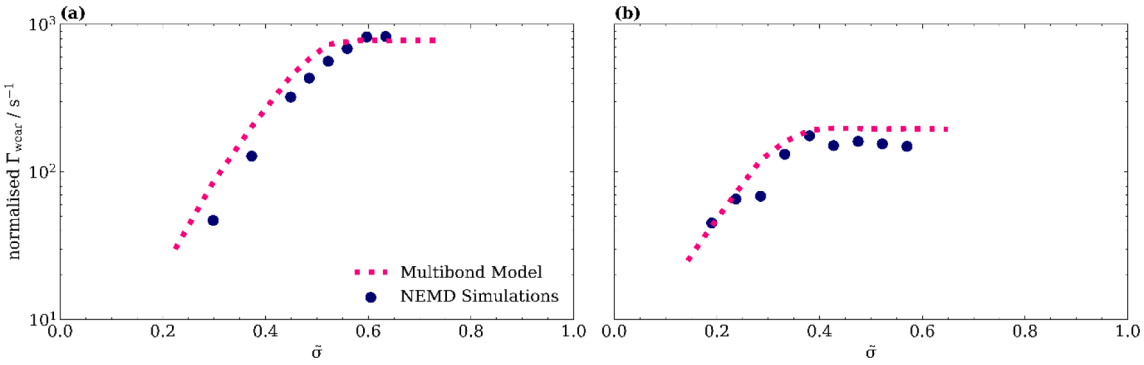

Fig. 8. Normalized atom wear rate (i.e., number of atoms removed from the asperity per unit time normalized by the estimated number of atoms in contact) as a function of dimensionless effective normal stress for the dry system at 500 K (a) and the wet system at 1000 K (b). The multibond wear model (Equation (8)) [16] is fit to the full data set. The σ values are calculated using Equation (9), with the normal stress calculated using the atoms in contact method based on the number of interfacial bonds.

The calculated wear rates are normalized by the average number of atoms in contact to account for the changing geometry of the asperity. The following model parameters were all determined from the NEMD simulations: $\Delta U = 69$ kJ mol^{-1} and 162 kJ mol^{-1} (C-O interfacial bond formation), $\Delta E_{off} = 66$ kJ mol^{-1} and 148 kJ mol^{-1} (C-O wearless rupture), $\Delta E_{wear} = 71$ kJ mol^{-1} and 133 kJ mol^{-1} (C-C wear), $\Delta V^{\ddagger} = 1.4$ Å^3 and 1.3 Å^3 (C-C wear), for the dry and wet systems, respectively. The bond-breaking length, $l_{break} = 3.0$ Å, was taken from the original frictional model [101].

Fig. 8 illustrates how the multibond wear model can be used to fit the initial wear data from our NEMD simulation over the entire load range studied. At low normal stress, standard SATA models hold since there is an exponential increase in the normalised wear rate with effective normal stress. There is then a transition region before, at high stress, the normalised wear rate becomes independent of normal stress. Here, bond formation is no longer the rate-limiting step for the wear process and thus standard SATA models break down [16]. While several other nanoscale wear models exist, they were unable to fully describe the initial wear rate data presented above. We also plotted the same data as shown in Fig. 8 but with the normal stress determined using the Hertz equation, as shown in the Supporting Information (Fig. S12).

3.4. Wear models (steady-state)

After the initial running-in phase (100 nm of sliding), a steady-state wear phase begins in which wear becomes almost linearly dependant on sliding distance, as shown in Fig. 2. Here, as well as atom-by-atom attrition, cluster detachment via tail fracture occurs [13], as can be seen in the snapshots in Fig. S3. This implies a crossover from short sliding distances, where wear processes that can be described by SATA models, to longer sliding distances where they can be approximated using the Archard model. Moreover, Fig. 2 shows that the steady-state wear rate is essentially independent of temperature, which is consistent with the Archard model, but not SATA models [102]. It should be noted, however, that the physicochemical mechanisms leading to wear are not consistent with those proposed in the Archard model, even at long sliding times.

To further test the applicability of the Archard model during the steady-state phase, we analysed the load-dependence of the wear rate, which should be linear. Fig. 9 shows the variation for the normalised wear rate, dW/dL, versus normal load F_N for the dry and wet system, where W is the worn volume per unit area (m^3/m^2) and L is sliding distance (m). The steady-state wear rates were estimated using linear fits to the wear versus time data for the dry (Fig. 2) and wet (Fig. S6) systems after 100 nm of sliding. The linearity of dW/dL as a function of F_N further suggets that the Archard model is applicable at the nanoscale. [6] This finding is consistent with previous NEMD simulations of wear in DLC-

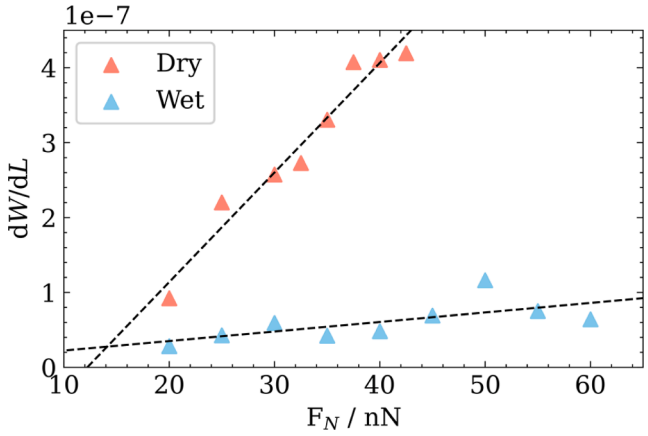

Fig. 9. The normalised wear rate, dW/dL, versus normal load, F_N, for the dry system at 500 K and the wet system at 1000 K. Steady-state wear rates are calculated from linear fits through the wear versus time data shown in Fig. 2 (dry) and Fig. S6 (wet) after the running-in period (sliding distance > 100 nm). Black dashed lines are linear fits through the data as predicted by the Archard model.

DLC contacts [13]. However, it is in disagreement with previous AFM experiments [10–12] that showed the non-linearity of wear as a function of both sliding distance and applied force. These differences could be due to the much lower sliding velocities in the experiments than the NEMD simulations [13]. On the other hand, Maw et al. [80] showed that contaminants including oxides and other chemical species present in AFM experimental studies could lead to non-linearity in the wear versus time behaviour, which the surfaces in our simulations are free from.

Wear during the initial 100 nm of sliding can be attributed to atom-by-atom attrition that be explained using the multibond model. From this point onwards, cluster detachment via tail fracture also occurs, as detailed by Sha et al. [13]. They noted that the average cluster size increased and few isolated atoms were lost at higher normal loads [13]. Diffusion of the carbon atoms into the α-quartz substrate and the formation of CO_2 in our simulations makes quantification of the cluster size more difficult in our simulations. However, the snapshots in Fig. S3 do seem to show an increase in cluster size with increasing normal load (and temperature). At high temperatures and loads, significant lateral atom migration takes place towards the trailing edge of the sliding asperity. Thus, it might be expected that longer simulations would lead to detachment of larger clusters.

Yoshino et al. [103] experimentally measured the wear rates of single-crystal diamond on quartz glass at 300 K. They found that the wear rate was significantly reduced when using water as a lubricant

[103], which is consistent with our NEMD simulation results for diamond on α-quartz contacts shown in Fig. 9. Due to the considerable computational expense of our NEMD simulations, a much higher sliding velocity (100 m s^{-1}) was required compared to the experiments (3×10^{-4} m s^{-1}) and the sliding distance was also smaller in the simulations (4×10^{-7} m) than the experiments (5×10^{-3} m). The normalised wear rates from the experiments, dW/dL, varied considerably with indentation depth (2–38 nm) between 1.1×10^{-6} and 1.6×10^{-7}. Thus, the normalised wear rates from our NEMD simulations (indentation depth ≈ 1 nm) for the dry (1×10^{-7} to 5×10^{-7}) and wet (2×10^{-8} to 1×10^{-7}) systems are close to the range observed experimentally. The wear rate is approximately one order of magnitude higher in the dry diamond-quartz system than when water molecules are present at the sliding interface, which is similar to the difference noted in previous experiments [84]. The corresponding wear coefficient, K_b, values from the Archard model (Equation (1)) are $5.0 \pm 0.3 \times 10^{-4}$ for the dry system and $7.1 \pm 2.7 \times 10^{-7}$ for the wet system. These values are close to experimental estimates of the wear coefficient in the Archard model for a diamond AFM tip sliding on a silicon nitride substrate ($K_b \approx 10^{-5}$–10^{-6}) [104], which will quickly oxidize when exposed to air and form an outer silica layer [105].

In summary, the Archard model, the standard SATA model and the non-empirical wear model are unable to describe the initial wear behaviour of our system at the highest loads studied in our NEMD simulations. The multibond model, which considers the formation and rupture of interfacial bonds, as well as rupture of bonds withing the sliding tip, can be used to fit the initial wear data from our NEMD simulation over the entire load range studied. After the running-in phase, the wear volume becomes almost linearly proportional to the sliding distance and applied load, suggesting that the Archard wear model can be used to empirically describe the wear behaviour even in these nanoscale simulations. However, the physicochemical processes observed in the simulations are not consistent with those assumed in the Archard model.

4. Conclusion

We have used NEMD simulations to quantify the early stages of the tribochemical wear of diamond tips sliding on α-quartz substrates. Our results show that diamond wear on α-quartz is initiated by the formation of C-O interfacial bonds, which is followed by C-C cleavage, and either diffusion of carbon into the substrate or further oxidation to form CO_2 molecules. Amorphization of the diamond tip also occurs during sliding, but this is not essential for wear to occur. The increase in wear rate with normal stress cannot be described using standard SATA-based models at high loads. However, the multibond wear model, which encapsulates three distinct SATA processes, is able to describe the initial wear behaviour of diamond on α-quartz over the entire load range studied. When the normal stress reaches a certain threshold, there is a transition from exponential growth of the initial wear rate with stress (as predicted by SATA models), towards stress-independent initial wear rate (as predicted by the Archard model). After the initial running-in period, tail fracture and cluster detachment occur as well as atom-by-atom attrition. Here, wear becomes approximately linearly proportional with sliding distance and load, which is consistent with the Archard model. The normalised wear rates obtained from the NEMD simulations are in good agreement with previous experiments. When water molecules are included inside the contact, interfacial bonding and wear were both significantly reduced due to passivation at the sliding interface. The multibond model can also be used to describe the initial wear behaviour for water-containing systems, but with a lower plateau wear rate. Thus, our results suggest that mitigation of interfacial bonding should be an effective strategy to improve tribological performance of bits for rock drilling.

CRediT authorship contribution statement

Jagjeevan S. Bhamra: Investigation, Methodology, Software, Formal analysis, Visualization, Writing – original draft. **James P. Ewen:** Conceptualization, Supervision, Project administration, Funding acquisition, Writing – review & editing. **Carlos Ayestarán Latorre:** Methodology, Software, Formal analysis, Writing – review & editing. **John A. R. Bomidi:** Supervision, Project administration, Funding acquisition, Writing – review & editing. **Marc W. Bird:** Project administration, Funding acquisition, Writing – review & editing. **Daniele Dini:** Conceptualization, Supervision, Project administration, Funding acquisition, Writing – review & editing.

Declaration of Competing Interest

The authors declare the following financial interests/personal relationships which may be considered as potential competing interests: James P. Ewen reports financial support was provided by Royal Academy of Engineering. Daniele Dini reports financial support was provided by Royal Academy of Engineering. Daniele Dini reports financial support was provided by Engineering and Physical Sciences Research Council. Jagjeevan S. Bhamra reports financial support was provided by Baker Hughes.

Data availability

Data will be made available on request.

Acknowledgements

J.S.B. thanks Baker Hughes for Ph.D. funding. J.P.E. thanks the Royal Academy of Engineering (RAEng) for a Research Fellowship. D.D. also acknowledges support via his Shell/RAEng Research Chair in Complex Engineering Interfaces. D.D. and J.P.E. thank the Engineering and Physical Sciences Research Council (EPSRC) for an Established Career Fellowship EP/N025954/1 and grant EP/P030211/1. We acknowledge the use of the Research Computing Service at Imperial College London (DOI:10.14469/hpc/2232) and the UK Materials and Molecular Modelling Hub, which is partially funded by EPSRC grant EP/T022213/1, EP/W032260/1 and EP/P020194/1.

Appendix A. Supplementary data

Supplementary data to this article can be found online at https://doi.org/10.1016/j.apsusc.2023.158152.

References

[1] W. Zhai, L. Bai, R. Zhou, X. Fan, G. Kang, Y. Liu, K. Zhou, Recent progress on wear-resistant materials: designs, properties, and applications, Adv. Sci. 8 (2021) 2003739.
[2] L. Mattei, F. Di Puccio, B. Piccigallo, E. Ciulli, Lubrication and wear modelling of artificial hip joints: a review, Tribol. Int. 44 (2011) 532–549.
[3] N.N. Gosvami, J.A. Bares, F. Mangolini, A.R. Konicek, D.G. Yablon, R.W. Carpick, Mechanisms of antiwear tribofilm growth revealed in situ by single-asperity sliding contacts, Science 348 (2015) 102–106.
[4] J.T. Burwell, Survey of possible wear mechanisms, Wear 1 (1957) 119–141.
[5] H.C. Meng, K.C. Ludema, Wear models and predictive equations: their form and content, Wear 181–183 (1995) 443–457.
[6] J.F. Archard, Contact and rubbing of flat surfaces, J. Appl. Phys. 24 (1953) 981.
[7] J.J. Kauzlarich, J.A. Williams, Archard wear and component geometry, Proc. Inst. Mech. Eng. Part J 215 (2001) 387–398.
[8] Y. Wang, J. Xu, Y. Ootani, N. Ozawa, K. Adachi, M. Kubo, Non-empirical law for nanoscale atom-by-atom wear, Adv. Sci. 8 (2020) 2002827.
[9] B. Gotsmann, M.A. Lantz, Atomistic wear in a single asperity sliding contact, Phys. Rev. Lett. 101 (2008), 125501.
[10] H. Bhaskaran, B. Gotsmann, A. Sebastian, U. Drechsler, M.A. Lantz, M. Despont, P. Jaroenapibal, R.W. Carpick, Y. Chen, K. Sridharan, Ultralow nanoscale wear through atom-by-atom attrition in silicon-containing diamond-like carbon, Nat. Nanotechnol. 5 (2010) 181–185.

[11] T.D.B. Jacobs, R.W. Carpick, Nanoscale wear as a stress-assisted chemical reaction, Nat. Nanotechnol. 8 (2013) 108–112.
[12] T.D.B. Jacobs, B. Gotsmann, M.A. Lantz, R.W. Carpick, On the application of transition state theory to atomic-scale wear, Tribol. Lett. 39 (2010) 257–271.
[13] Z.-D. Sha, V. Sorkin, P.S. Branicio, Q.-X. Pei, Y.-W. Zhang, D.J. Srolovitz, Large-scale molecular dynamics simulations of wear in diamond-like carbon at the nanoscale at the nanoscale, Appl. Phys. Lett. 27 (2013), 073118.
[14] J. Liu, Y. Jiang, D.S. Grierson, K. Sridharan, Y. Shao, T.D.B. Jacobs, M.L. Falk, R. W. Carpick, K.T. Turner, Tribochemical wear of diamond-like carbon-coated atomic force microscope tips, ACS Appl. Mater. Interfaces 9 (2017) 35341–35348.
[15] Y. Mo, K.T. Turner, I. Szlufarska, Friction laws at the nanoscale, Nature 457 (2009) 1116–1119.
[16] Y. Shao, T.D.B.B. Jacobs, Y. Jiang, K.T. Turner, R.W. Carpick, M.L. Falk, Multibond model of single-asperity tribochemical wear at the nanoscale, ACS Appl. Mater. Interfaces 9 (2017) 35333–35340.
[17] A.E. Filippov, J. Klafter, M. Urbakh, Friction through dynamical formation and rupture of molecular bonds, Phys. Rev. Lett. 92 (2004), 135503.
[18] H.K. Tönshoff, H. Hillmann-Apmann, J. Asche, Diamond tools in stone and civil engineering industry: cutting principles, wear and applications, Diam. Relat. Mater. 11 (2002) 736–741.
[19] R.H. Wentorf, R.C. DeVries, F.P. Bundy, Sintered superhard materials, Science 208 (1980) 873–880.
[20] F.C. Appl, C.C. Wilson, I. Lakshman, F.C. Appl, C.C. Wilson, I. Lakshman, Measurement of forces, temperatures and wear of PDC cutters in rock cutting, Wear 169 (1993) 9–24.
[21] M.E. Hossain, Drilling costs estimation for hydrocarbon wells, J. Sustain. Energy Eng. 3 (2015) 3–32.
[22] A. Ersoy, M.D. Waller, Wear characteristics of PDC pin and hybrid core bits in rock drilling, Wear 188 (1995) 150–165.
[23] M. Yahiaoui, L. Gerbaud, J.Y. Paris, J. Denape, A. Dourfaye, A study on PDC drill bits quality, Wear 298–299 (2013) 32–41.
[24] M. Yahiaoui, J.Y. Paris, K. Delbé, J. Denape, L. Gerbaud, C. Colin, O. Ther, A. Dourfaye, Quality and wear behavior of graded polycrystalline diamond compact cutters, Int. J. Refract. Met. Hard Mater. 56 (2016) 87–95.
[25] C. Wang, S. Li, L. Zhang, Evaluation of rock abrasiveness class based on the wear mechanisms of PDC cutters, J. Pet. Sci. Eng. 174 (2019) 959–967.
[26] D.W. Wheeler, Applications of diamond to improve tribological performance in the oil and gas industry, Lubricants 6 (2018) 84.
[27] U. Beste, A. Lundvall, S. Jacobson, Micro-scratch evaluation of rock types - a means to comprehend rock drill wear, Tribol. Int. 37 (2004) 203–210.
[28] A. Ortega, D.A. Glowka, Frictional heating and convective cooling of polycrystalline diamond drag tools during rock cutting, Soc. Pet. Eng. J. 24 (1984) 121–128.
[29] P.A. Bex, G.R. Shafto, The influence of temperature and heating time on PCD performance, Ind. Diam. Div. Commun. 44 (1978) 128–132.
[30] E. Rabinowicz, Abrasive wear resistance as a materials test, Lubr. Eng. 33 (1977) 378–381.
[31] M.T. Hamzaban, J. Rostami, F. Dahl, F.J. Macias, P.D. Jakobsen, Wear of cutting tools in hard rock excavation process: a critical review of rock abrasiveness testing methods, Rock Mech. Rock Eng. 1 (2022) 3.
[32] E.L.H. Thomas, G.W. Nelson, S. Mandal, J.S. Foord, O.A. Williams, Chemical mechanical polishing of thin film diamond, Carbon N. Y. 68 (2014) 473–479.
[33] A. Peguiron, G. Moras, M. Walter, H. Uetsuka, L. Pastewka, M. Moseler, Activation and mechanochemical breaking of C-C bonds initiate wear of diamond (110) surfaces in contact with silica, Carbon. 98 (2016) 474–483.
[34] A. Mir, X. Luo, J. Sun, The investigation of influence of tool wear on ductile to brittle transition in single point diamond turning of silicon, Wear 364–365 (2016) 233–243.
[35] P. Jia, M. Zhou, Tool wear and its effect on surface roughness in diamond cutting of glass soda-lime, Chinese J. Mech. Eng. 25 (2012) 1224–1230.
[36] A.G. Khurshudov, K. Kato, H. Koide, Nano-wear of the diamond AFM probing tip under scratching of silicon, studied by AFM, Tribol. Lett. 2 (1996) 345–354.
[37] A.C.T. van Duin, S. Dasgupta, F. Lorant, W.A. Goddard III, ReaxFF: A reactive force field for hydrocarbons, J. Phys. Chem. A 105 (2001) 9396–9409.
[38] S.J. Plimpton, A.P. Thompson, Computational aspects of many-body potentials, MRS Bull. 37 (2012) 513–521.
[39] T.P. Senftle, S. Hong, M.M. Islam, S.B. Kylasa, Y. Zheng, Y.K. Shin, C. Junkermeier, R. Engel-Herbert, M.J. Janik, H.M. Aktulga, T. Verstraelen, A. Grama, A.C.T. Van Duin, The ReaxFF reactive force-field: development, applications and future directions, npj Comput. Mater. 2 (2016).
[40] A. Martini, S.J. Eder, N. Dörr, Tribochemistry: A review of reactive molecular dynamics simulations, Lubricants 8 (2020) 44.
[41] D.A. Newsome, D. Sengupta, H. Foroutan, M.F. Russo, A.C.T. Van Duin, Oxidation of silicon carbide by O_2 and H_2O: A ReaxFF reactive molecular dynamics study, Part I, J. Phys. Chem. C 116 (2012) 16111–16121.
[42] J.S. Bhamra, J.P. Ewen, C.A. Latorre, J.A.R. Bomidi, M.W. Bird, N. Dasgupta, A.C. T. van Duin, D. Dini, Interfacial bonding controls friction in diamond-rock contacts, J. Phys. Chem. C 125 (2021) 18395–18408.
[43] P. Lai, K. Moulton, S. Krevor, Pore-scale heterogeneity in the mineral distribution and reactive surface area of porous rocks, Chem. Geol. 411 (2015) 260–273.
[44] I. Van der Molen, The shift of the α-β transition temperature of quartz associated with the thermal expansion of granite at high pressure, Tectonophysics 73 (1981) 323–342.
[45] N.H. De Leeuw, F.M. Higgins, S.C. Parker, Modeling the surface structure and stability of α-quartz, J. Phys. Chem. B 103 (1999) 1270–1277.
[46] D.C. Yue, T.B. Ma, Y.Z. Hu, J. Yeon, A.C.T. van Duin, H. Wang, J. Luo, Tribochemical mechanism of amorphous silica asperities in aqueous environment: a reactive molecular dynamics study, Langmuir 31 (2015) 1429–1436.
[47] R.M. Pashley, J.A. Kitchener, Surface forces in adsorbed multilayers of water on quartz, J. Colloid Interface Sci. 71 (1979) 491–500.
[48] J. Yang, E.G. Wang, Water adsorption on hydroxylated α -quartz (0001) surfaces: from monomer to flat bilayer, Phys. Rev. B - Condens. Matter Mater. Phys. 73 (2006), 035406.
[49] A.C.T.T. Van Duin, S. Dasgupta, F. Lorant, W.A. Goddard, W.A. Goddard III, ReaxFF: A reactive force field for hydrocarbons, J. Phys. Chem. A 105 (2001) 9396–9409.
[50] A.P. Thompson, H.M. Aktulga, R. Berger, D.S. Bolintineanu, W.M. Brown, P. S. Crozier, P.J. in 't Veld, A. Kohlmeyer, S.G. Moore, T.D. Nguyen, R. Shan, M. J. Stevens, J. Tranchida, C. Trott, S.J. Plimpton, LAMMPS - a flexible simulation tool for particle-based materials modeling at the atomic, meso, and continuum scales, Comput. Phys. Commun. 271 (2022), 108171.
[51] K. Chenoweth, A.C.T.T. Van Duin, W.A. Goddard, W.A. Goddard III, ReaxFF reactive force field for molecular dynamics simulations of hydrocarbon oxidation, J. Phys. Chem. A 112 (2008) 1040–1053.
[52] H.M. Aktulga, J.C. Fogarty, S.A. Pandit, A.Y. Grama, Parallel reactive molecular dynamics: numerical methods and algorithmic techniques, Parallel Comput. 38 (2012) 245–259.
[53] A.K. Rappé, W.A. Goddard, Charge equilibration for molecular dynamics simulations, J. Phys. Chem. 95 (1991) 3358–3363.
[54] A. Nakano, Parallel multilevel preconditioned conjugate-gradient approach to variable-charge molecular dynamics, Comput. Phys. Commun. 104 (1997) 59–69.
[55] M.J. Buehler, A.C.T. van Duin, W.A. Goddard III, Multiparadigm modeling of dynamical crack propagation in silicon using a reactive force field, Phys. Rev. Lett. 96 (2006), 095505.
[56] A.C.T. Van Duin, A. Strachan, S. Stewman, Q. Zhang, X. Xu, W.A. Goddard, ReaxFFSiO reactive force field for silicon and silicon oxide systems, J. Phys. Chem. A 107 (2003) 3803–3811.
[57] J.C. Fogarty, H.M. Aktulga, A.Y. Grama, A.C.T. van Duin, S.A. Pandit, A reactive molecular dynamics simulation of the silica-water interface, J. Chem. Phys. 132 (2010), 174704.
[58] K. Chenoweth, S. Cheung, A.C.T. van Duin, W.A. Goddard III, E.M. Kober, Simulations on the thermal decomposition of a poly(dimethylsiloxane) polymer using the ReaxFF reactive force field, J. Am. Chem. Soc. 127 (2005) 7192–7202.
[59] B.D. Jensen, K.E. Wise, G.M. Odegard, Simulation of the elastic and ultimate tensile properties of diamond, graphene, carbon nanotubes, and amorphous carbon using a revised ReaxFF parametrization, J. Phys. Chem. A 119 (2015) 9710–9721.
[60] Z.B. Milne, J.D. Schall, T.D.B. Jacobs, J.A. Harrison, R.W. Carpick, Covalent bonding and atomic-level plasticity increase adhesion in silicon-diamond nanocontacts, ACS Appl. Mater. Interfaces 11 (2019) 40734–40748.
[61] S. Kumar, D. Parks, K. Kamrin, Mechanistic origin of the ultrastrong adhesion between graphene and A-SiO2: beyond van der waals, ACS Nano 10 (2016) 6552–6562.
[62] S. Nouranian, S.R. Gwaltney, M.I. Baskes, M.A. Tschopp, M.F. Horstemeyer, Simulations of tensile bond rupture in single alkane molecules using reactive interatomic potentials, Chem. Phys. Lett. 635 (2015) 278–284.
[63] C. Tomas, De, A. Aghajamali, J.L. Jones, D.J. Lim, I. Suarez-martinez, N.A. Marks, J.L. Maria, C. de Tomas, A. Aghajamali, J.L. Jones, D.J. Lim, M.J. López, I. Suarez-martinez, N.A. Marks, Transferability in interatomic potentials for carbon, Carbon N. Y. 155 (2019) 624–634.
[64] Y. Wang, N. Yamada, J. Xu, J. Zhang, Q. Chen, Y. Ootani, Y. Higuchi, N. Ozawa, M.D.B. Bouchet, J.M. Martin, S. Mori, K. Adachi, M. Kubo, Triboemission of hydrocarbon molecules from diamond-like carbon friction interface induces atomic-scale wear, Sci. Adv. 5 (2019) 1–10.
[65] H. Wang, Y. Ge, L. Shi, Technologies in deep and ultra-deep well drilling: present status, challenges and future trend in the 13th five-year plan period (2016–2020), Nat. Gas Ind. B 4 (2017) 319–326.
[66] P.S.M. Dougherty, R. Pudjoprawoto, C.F. Higgs III, Bit cutter-on-rock tribometry: analyzing friction and rate-of-penetration for deep well drilling substrates, Tribol. Int. 77 (2014) 178–185.
[67] L.C. Verlet, "Experiments" on classical fluids. I. thermodynamical properties of lennard-jones molecules, Phys. Rev. 159 (1967) 98.
[68] T. Schneider, E. Stoll, Molecular-dynamics study of a three-dimensional one-component model for distortive phase transitions, Phys. Rev. B 17 (1978) 1302.
[69] A. Stukowski, Visualization and analysis of atomistic simulation data with OVITO-the open visualization tool, Model. Simul. Mater. Sci. Eng. 18 (2010), 015012.
[70] B. Luan, M.O. Robbins, The breakdown of continuum models for mechanical contacts, Nature 435 (2005) 929–932.
[71] T.D.B. Jacobs, A. Martini, Measuring and understanding contact area at the nanoscale: a review, Appl. Mech. Rev. 69 (2017), 060802.
[72] Y. Wang, J. Qin, J. Xu, J. Sun, L. Chen, L. Qian, M. Kubo, Definition of atomic-scale contact: what dominates the atomic-scale friction behaviors? Langmuir 38 (2022) 11699–11706.
[73] M.C. Pitman, A.C.T. van Duin, Dynamics of confined reactive water in smectite clay-zeolite composites, J. Am. Chem. Soc. 134 (2012) 3042–3053.
[74] J.P. Ewen, C. Ayestarán Latorre, C. Gattinoni, A. Khajeh, J.D. Moore, J.E. Remias, A. Martini, D. Dini, Substituent effects on the thermal decomposition of phosphate esters on ferrous surfaces, J. Phys. Chem. C 124 (2020) 9852–9865.

[75] E. Paul, C.J. Evans, A. Mangamelli, M.L. McGlauflin, R.S. Polvani, Chemical aspects of tool wear in single point diamond turning, Precis. Eng. 18 (1996) 4–19.
[76] C. Köhler, Z. Hajnal, T. Frauenheim, P. Deák, S. Suhai, Theoretical investigation of carbon defects and diffusion in α-quartz, Phys. Rev. B 64 (2001), 085333.
[77] D.A. Rigney, S. Karthikeyan, The evolution of tribomaterial during sliding: a brief introduction, Tribol. Lett. 39 (2010) 3–7.
[78] L. Pastewka, S. Moser, P. Gumbsch, M. Moseler, Anisotropic mechanical amorphization drives wear in diamond, Nat. Mater. 10 (2011) 34–38.
[79] X. Hu, M.V.P. Altoe, A. Martini, Amorphization-assisted nanoscale wear during the running-in process, Wear 370–371 (2017) 46–50.
[80] W. Maw, F. Stevens, S.C. Langford, J.T. Dickinson, Single asperity tribochemical wear of silicon nitride studied by atomic force microscopy, J. Appl. Phys. 92 (2002) 5103–5109.
[81] P.E. Sheehan, The wear kinetics of NaCl under dry nitrogen and at low humidities, Chem. Phys. Lett. 410 (2005) 151–155.
[82] Q. Lin, S. Chen, Z. Ji, Z. Huang, Z. Zhang, B. Shen, High-temperature wear mechanism of diamond at the nanoscale: a reactive molecular dynamics study, Appl. Surf. Sci. 585 (2022), 152614.
[83] V.A. Mukhanov, O.O. Kurakevych, V.L. Solozhenko, Hardness of materials at high temperature and high pressure, Philos. Mag. 89 (2010) 2117–2127.
[84] F.P. Bowden, H.G. Scott, The polishing, surface flow and wear of diamond and glass, Proc. R. Soc. London. Ser. A. Math. Phys. Sci. 248 (1958) 368–378.
[85] J. Yeon, A.C.T. van Duin, S.H. Kim, Effects of water on tribochemical wear of silicon oxide interface: molecular dynamics (MD) study with reactive force field (ReaxFF), Langmuir 32 (2016) 1018–1026.
[86] M. Wang, F. Duan, X. Mu, Effect of surface silanol groups on friction and wear between amorphous silica surfaces, Langmuir 35 (2019) 5463–5470.
[87] M. Cutini, G. Forghieri, M. Ferrario, M.C. Righi, Adhesion, friction and tribochemical reactions at the diamond-silica interface, Carbon N. Y. 203 (2023) 601–610.
[88] P.J. Blau, On the nature of running-in, Tribol. Int. 38 (2005) 1007–1012.
[89] K. Wang, J. Zhang, T. Ma, Y. Liu, A. Song, X. Chen, Y. Hu, R.W. Carpick, J. Luo, Unraveling the friction evolution mechanism of diamond-like carbon film during nanoscale running-in process toward superlubricity, Small 17 (2021) 2005607.
[90] H. Spikes, Stress-augmented thermal activation: tribology feels the force, Friction 6 (2018) 1–31.
[91] J. Zhang, J.P. Ewen, M. Ueda, J.S.S. Wong, H.A. Spikes, Mechanochemistry of zinc dialkyldithiophosphate on steel surfaces under elastohydrodynamic lubrication conditions, ACS Appl. Mater. Interfaces 12 (2020) 6662–6676.
[92] F.H. Bhuiyan, S.H. Kim, A. Martini, Reactive molecular dynamics simulations of thermal and shear-driven oligomerization, Appl. Surf. Sci. 591 (2022), 153209.
[93] M. Vorholzer, J.G. Vilhena, R. Perez, E. Gnecco, D. Dietzel, A. Schirmeisen, Temperature activates contact aging in silica nanocontacts, Phys. Rev. X 91 (2019), 041045.
[94] V. Vahdat, K.E. Ryan, P.L. Keating, Y. Jiang, S.P. Adiga, J.D. Schall, K.T. Turner, J.A. Harrison, R.W. Carpick, Atomic-scale wear of amorphous hydrogenated carbon during intermittent contact: a combined study using experiment, simulation, and theory, ACS Nano 8 (2014) 7027–7040.
[95] G. Davies, T. Evans, Graphitization of diamond at zero pressure and at a high pressure, Proc. R. Soc. London. A. Math. Phys. Sci. 328 (1972) 413–427.
[96] A. Martini, S.H. Kim, Activation volume in shear-driven chemical reactions, Tribol. Lett. 69 (2021) 1–14.
[97] J. Qian, C. Pantea, J. Huang, T.W. Zerda, Y. Zhao, Graphitization of diamond powders of different sizes at high pressure-high temperature, Carbon N. Y. 42 (2004) 2691–2697.
[98] Q. Sun, M. Alam, Relative oxidation behavior of chemical vapor deposited and type ii a natural diamonds, J. Electrochem. Soc. 139 (1992) 933–936.
[99] S.R. Kelemen, H. Freund, A comparison of O2 and CO2 oxidation of glassy carbon surfaces, Carbon N. Y. 23 (1985) 723–729.
[100] Y. Yang, L. Huang, Y. Shi, Adhesion suppresses atomic wear in single-asperity sliding, Wear 352–353 (2016) 31–41.
[101] I. Barel, M. Urbakh, L. Jansen, A. Schirmeisen, Multibond dynamics of nanoscale friction: the role of temperature, Phys. Rev. Lett. 104 (2010) 66104–66108.
[102] Y. Yang, C.S. O'Hern, L. Huang, Y. Shi, The nature of atomic wear from molecular simulations, Tribol. Int. 167 (2022), 107418.
[103] M. Yoshino, S. Nakajima, M. Terano, Tool wear of a single-crystal diamond tool in nano-groove machining of a quartz glass plate, Surf. Topogr. Metrol. Prop. 3 (2015), 044007.
[104] K.H. Chung, D.E. Kim, Wear characteristics of diamond-coated atomic force microscope probe, Ultramicroscopy 108 (2007) 1–10.
[105] S.I. Raider, R. Flitsch, J.A. Aboaf, W.A. Pliskin, Surface oxidation of silicon nitride films, J. Electrochem. Soc. 123 (1976) 560–565.